

Effect of thickness and build direction on the mechanical behavior and microstructure of AISI 316L stainless steel produced by Laser Beam Powder Bed Fusion

Evren Yasa^{1*}, Mutlu Karasoglu²

¹*Eskisehir Osmangazi University, Mechanical Engineering, Buyukdere Mah. Prof. Dr. Nabi Avci Blv. No: 4, TR-26040 Odunpazarı/Eskisehir, Turkey*

²*Eskisehir Technical University, Mechanical Engineering, 2 Eylül Kampusu, TR-26555 Tepebaşı/Eskisehir, Turkey*

Received 3 September 2021, received in revised form 28 March 2022, accepted 28 March 2022

Abstract

Laser Beam Powder Bed Fusion (LB-PBF) is a metal additive manufacturing process with the highest technological maturity and industrial acceptance levels due to its main advantage of producing complex geometries. However, there are yet some barriers to overcome for the broader adoption of LB-PBF. One of them is the questionable part quality depending on various factors, including the specimen geometry and build orientation. Thus, this study aims to understand the effect of the build orientation and specimen thickness on the obtained microstructure and mechanical properties of AISI 316L samples in terms of tensile behavior and microhardness. As a result of this study, it is observed that the variation in microhardness of samples built in different orientations or with different thicknesses is negligible.

Moreover, the thickness of the tensile test specimen only affects the ductility mainly due to the statistically higher risk of a detrimental effect of the defects in the thinner specimens, whereas the build direction is more influential on the yield and ultimate tensile strength values leading to an approximate change of 15 % and anisotropic results. Vertically standing samples exhibit the lowest strength values among all build directions. The changes in the tensile properties are attributed to the microstructural effects, including grain size, morphology, and orientation.

Key words: Laser Beam Powder Bed Fusion, mechanical behavior, build direction, specimen thickness

1. Introduction

Laser Beam Powder Bed Fusion (LB-PBF) is one of the most promising industrial additive manufacturing (AM) technologies developed to produce complex shaped metal parts from powder feedstock [1]. In the LB-PBF process, a particular region of the powder bed in each layer is melted by a focused laser beam with a high energy density according to the three-dimensional Computer-Aided Design (CAD) model of the part to be produced. Laser scanning followed by a powder coating for each layer continues until the component production in the powder bed is completed [2]. Compared to other AM processes, LB-PBF serves many benefits, including the ability to process

a wide spectrum of materials, near net shape component production capability, relatively low cost, and high functionality [3]. In addition, LB-PBF is able to produce almost entirely dense parts with good mechanical properties, and only a limited amount of waste material is generated due to its inherent nature [4]. On the other hand, LB-PBF has some disadvantages, including relatively low production speeds, high energy consumption, high initial investment costs, and high surface roughness necessitating post-processes for critical applications [3]. LB-PBF also suffers from mechanical and microstructural anisotropy due to directional solidification and thermal gradients inherent to the layerwise manner [5].

One of the most important parameters influenc-

*Corresponding author: e-mail address: evasa@ogu.edu.tr

ing the mechanical and microstructural anisotropy of the parts is the build orientation. In the study of Yadroitsev and Smurov, the mechanical properties of horizontally and vertically built samples from Inconel 625 are investigated. It was shown that horizontally built samples exhibited higher Young's modulus than vertically built samples which is attributed to a high number of layers of vertically built samples leading to a higher amount of interlayer defects [6]. Liverani et al. compared 90° and 45° build angles in AISI 316L stainless steel specimens, and they have reported that build direction changes crystallographic orientation. The samples with a 45° build angle displayed higher tensile strength and fatigue resistance [7]. Rakesh et al. assessed the build orientation effect on tensile and impact properties of AlSi10Mg samples. It was demonstrated that both tensile and impact resistance of transversely built samples were higher than longitudinal counterparts. Researchers have explained the superior mechanical performance of transversely built samples by higher density and lower surface roughness [8].

According to Menezes et al., the build direction has a significant impact on the tensile properties of A357, an age hardenable Al alloy. They have concluded that the melt pool boundaries act as preferential paths for crack propagation, and build orientation alters mechanical properties by changing the location of melt pool boundaries [9]. Ren et al. studied the effect of various build orientations (0-30-45-60-90°) on the tensile performance of LB-PBF Ti6Al4V and found that build orientation is the reason for differences in the tensile strength. They attributed the difference in the strength of the samples built in different directions to residual stresses and pore distribution [10]. Rötgers et al. addressed the mechanical properties obtained with the same AISI 316L stainless steel powder built horizontally and vertically on different machines. Although optimized parameters were used in each machine, significantly different densities and mechanical properties were obtained. Depending on the machine, the effect of the build direction varied, but anisotropy was observed in almost all tensile properties [11]. AISI 316L was also addressed by Ni et al. in terms of anisotropy in mechanical properties and corrosion resistance, and it was concluded that different build directions lead to a significant change in the microstructure leading to statistically different mechanical properties. Alsalla et al. also addressed the correlation between the microstructure and obtained mechanical properties of AISI 316L stainless steel processed in different build directions. Despite the high porosity (4%) and cracking problems, the tensile properties were better than their conventional counterparts. It was concluded that the build direction affected the fracture toughness; the z axis was the weakest [12]. Taufek et al. addressed AISI 316L

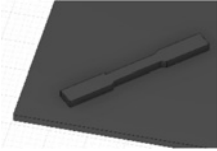
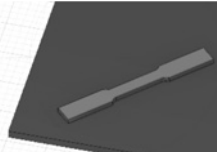
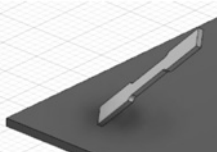
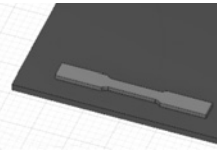
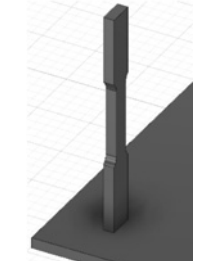
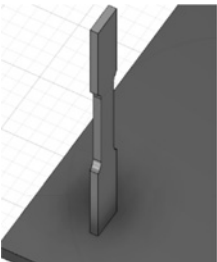
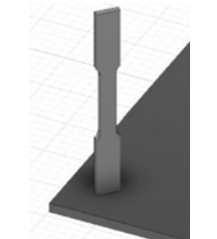
stainless steel parts produced by the LB-PBF process in three directions with tensile testing and microstructural investigations. The conclusion was that samples with perpendicular layer boundaries towards the direction of the load had lower mechanical properties than the parallel layer boundaries [13]. Delgado et al., in contrast to other studies, concluded that the build direction has a significant influence on the bending strength and elongation, with no effect on tensile strength [14]. Although there are many studies on the effect of the build direction on the mechanical properties of AISI 316L processed with the LB-PBF technology, these generally address only parts built horizontally or vertically. Moreover, the direction of the powder coating is not considered.

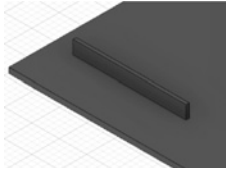
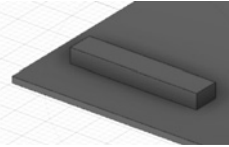
This study does not only investigate the effect of the build direction along with different directions but also aims to understand the effect of parameters that change the thermal history of the part, such as the specimen thickness. Thus, the effects of build direction concerning the powder coating direction and specimen thickness are addressed in this study by means of tensile properties, microhardness, and microstructure.

2. Materials and methods

In this study, several specimens were built by the LB-PBF process under different conditions to understand the effect of the build orientation and the specimen geometry in terms of production thickness. AISI 316L stainless steel powder was utilized with a particle size within the range of 15–45 μm . Samples were fabricated on an EOS M280 machine with a layer thickness of 30 μm and optimized LB-PBF parameters for maximum performance in terms of density and subsequent to LB-PBF, only high-temperature stress relief heat treatment (1000°C and 1 h) was applied to the samples. The experimental variables are shown in Table 1. The orientations of the specimens are shown by the rotational angles along the x , y , and z axes, i.e., α , β , and γ angles, respectively. The specimens were produced in two batches, with the batch numbers indicated in the same table. For each configuration in both batches, 5 repetitions of tensile testing were carried out. The orientation and geometry of the samples are demonstrated in Fig. 1. In the first batch, only horizontal specimens with a rotational angle of 45 degrees around the z -axis were produced in two thickness values of 5 and 3 mm, respectively, for Group 1_1 and Group 1_2. In the second batch, most specimens were produced with a thickness of 3 mm, e.g., Group 2_1, 2_2, 2_4, 2_5, and 2_6. In these specimens, the build orientations were changed. Group 2_3 was built in the same build direction as Group 2_2 but with a thickness of 5 mm, whereas Group 2_7 specimens were

Table 1. The study variables (specimen thickness and orientation)

Group #	Orientation on the build platform	α	β	γ	Final specimen thickness (mm)	Production batch #	Orientation schema
1_1	Horizontal lying specimens (in XY plane) B1_S1_90_45_0.5MM Net shape 1 mm offset	90°	0°	45°	5	1	
1_2	Horizontal lying specimens (in XY plane) B1_S2_90_45_0.3MM Net shape 1 mm offset	90°	0°	45°	3	1	
2_1	Inclined specimens B2_S1_45_45_0.3MM Net shape 1 mm offset	45°	45°	0°	3	2	
2_2	Horizontal lying specimens (in XY plane) B2_S2_0_90_0.3MM Net shape 1 mm offset	0°	90°	0°	3	2	
2_3	Vertical standing specimens (in ZY plane) B2_S3_0_0_0.5MM Net shape 1 mm offset	0°	0°	0°	5	2	
2_4	Vertical standing specimens (in ZY plane) B2_S4_0_0_0.3MM Net shape 1 mm offset	0°	0°	0°	3	2	
2_5	Vertical standing specimens B2_S5_0_0_45_0.3MM Net shape 1 mm offset	0°	0°	45°	3	2	

2_6	Vertical lying specimens B2_S6_0_90_90_3MM Rectangular prism (103 × 20 × 12 mm ³)	0°	90°	90°	3	2	
2_7	Vertical lying specimens B2_S6_0_90_90_3MM Rectangular prism (103 × 20 × 12 mm ³)	0°	90°	90°	3	2	

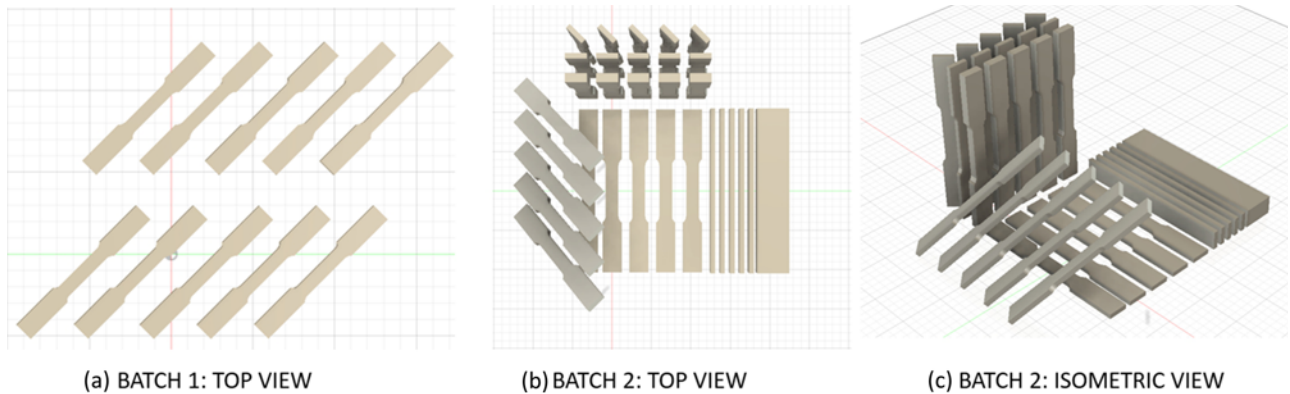


Fig. 1. Specimen orientations, from left to right: batch-1 top view, batch-2 top view, and batch-2 isometric view.

cut from a thick block produced with dimensions of $103 \times 20 \times 12 \text{ mm}^3$.

Tensile tests were performed with a Zwick-Roell Z300 testing machine at a speed of 20 mm min^{-1} with a maximum capacity of 300 kN according to the ASTM E8 standard [15]. The subsize specimen geometry with a width (W) of 6 mm was utilized per this standard. The thickness is allowed to vary depending on the material's nominal thickness to be tested. Thus, 3 and 5 mm thick specimens were tested in this study to understand if there is any difference in obtained mechanical properties. An ARAMIS 5M optical measurement system from GOM GmbH, with 2 5MP digital cameras is used to record the specimen surface during testing. Using the digital image correlation data processing method, the recordings obtained by the optical extensometer were processed with ARAMIS software to calculate the deformation. The offset method is used to determine the yield strength, and the slope of the elastic region is reported as Young's modulus.

Most of the specimens, except the sets numbered 2_6 and 2_7, were produced with an offset of 1 mm for further machining the circumference. Due to the expected residual stresses, the samples oriented at $\alpha = 0^\circ$, $\beta = 90^\circ$, and $\gamma = 90^\circ$ (see Set 2_6 in Table 1) were built as rectangular prisms with dimensions of

$103 \times 20 \times 12 \text{ mm}^3$ and later machined to final geometry.

The microstructure of the samples was investigated with optical microscopy (OM) after tensile testing from grip positions. Before microstructural investigations, bulk samples were ground with 1000, 2500, and 4000 grit SiC papers, respectively, and polished to $1 \mu\text{m}$ with a diamond solution. Before etching, the specimens were observed in terms of defects such as porosity and cracking. The porosity measurement procedure is presented in Fig. 2. After polishing, at least 3 images at different magnifications ($\times 5$, $\times 10$, $\times 20$) were captured from the specimens and were converted to black and white images using the same threshold value of 0.4. Using a simple programming code, the ratio of the number of black pixels to the total number of pixels is calculated as the porosity.

Electro-etching was performed with a 70% nitric acid solution at room temperature, using 1.5 V for etching times of between 10 and 20 s. Quantitative image analysis of microstructures was performed by using the FIJI software package. Grain boundaries and grains in the OM images were classified by the Trainable Weka Segmentation Fiji plugin. For classifications, a random forest classifier with 2 random features, 200 decision trees, 2 decimal places for computational accuracy, and 5 image filters (Gaussian blur,

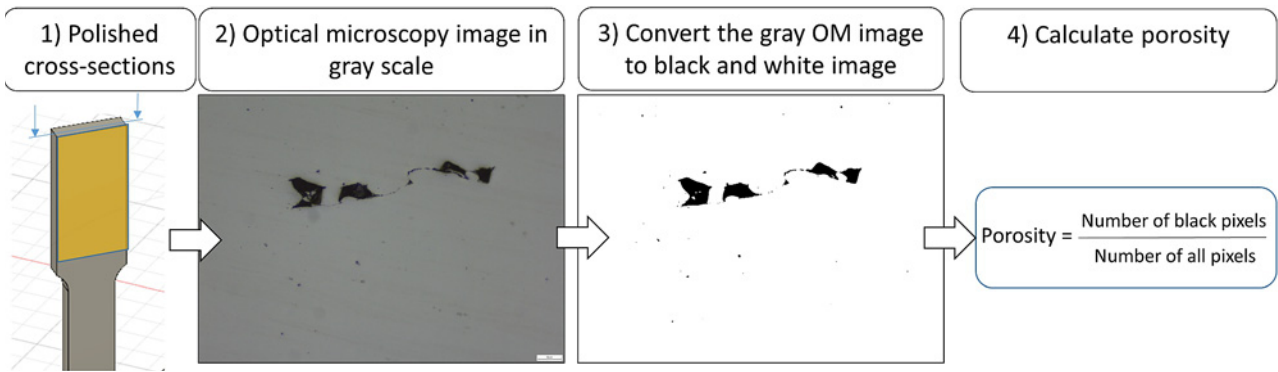


Fig. 2. Porosity measurement procedure.

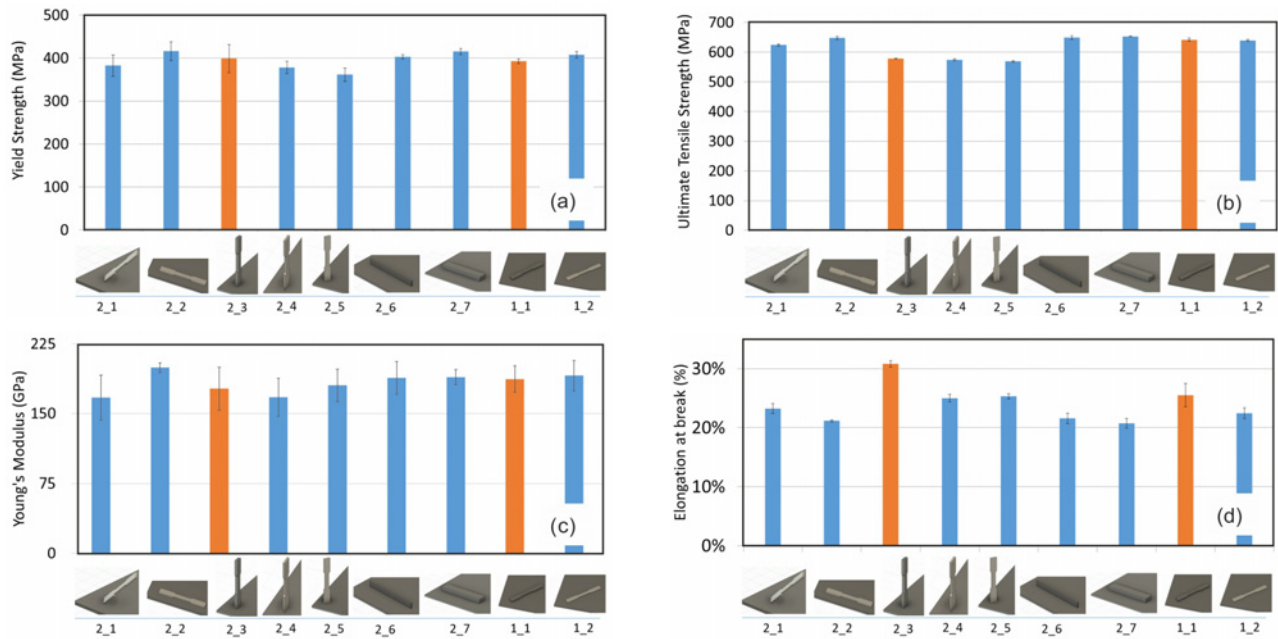


Fig. 3. Tensile test results in terms of (a) yield strength, (b) UTS, (c) Young’s modulus, and (d) elongation, where orange bars represent a final specimen thickness of 5 mm in contrast to specimens having a final thickness of 3 mm shown in blue.

Hessian matrix, Sobel, Gaussian distribution difference, and membrane projection) was utilized. After classification, the length of the scale bars in pixels was measured, and grain areas were calculated. Grain sizes were obtained by area-based estimation, which equals the diameter of the sphere that has the same area as a given individual grain. The aspect ratio of grains was acquired by dividing the longest length by the shortest grain length in the microstructure images.

The hardness measurement of bulk samples was conducted in accordance with ASTM E92-17 standard on a Future Tech FM700 testing equipment by using a Vickers diamond pyramid indenter under a test load of 100 gf [16].

3. Results

3.1. Tensile test results

The average tensile test results for each batch of 5 repetitions are presented in Fig. 3 with the calculated standard deviations. The orange bars in the figures depict a final specimen thickness of 5 mm, whereas the blue bars are the results of specimens having a final thickness of 3 mm built in different orientations.

The effect of specimen thickness is tested with group numbers of 1_1 versus 1_2 as well as 2_3 versus 2_4 for different orientations. Groups 2_3 and 2_4 are vertical standing specimens of which the long side of the cross-section is aligned with the coater direction, whereas groups 1_1 and 1_2 are horizontally lying coupons of which the long side has 45 degrees of

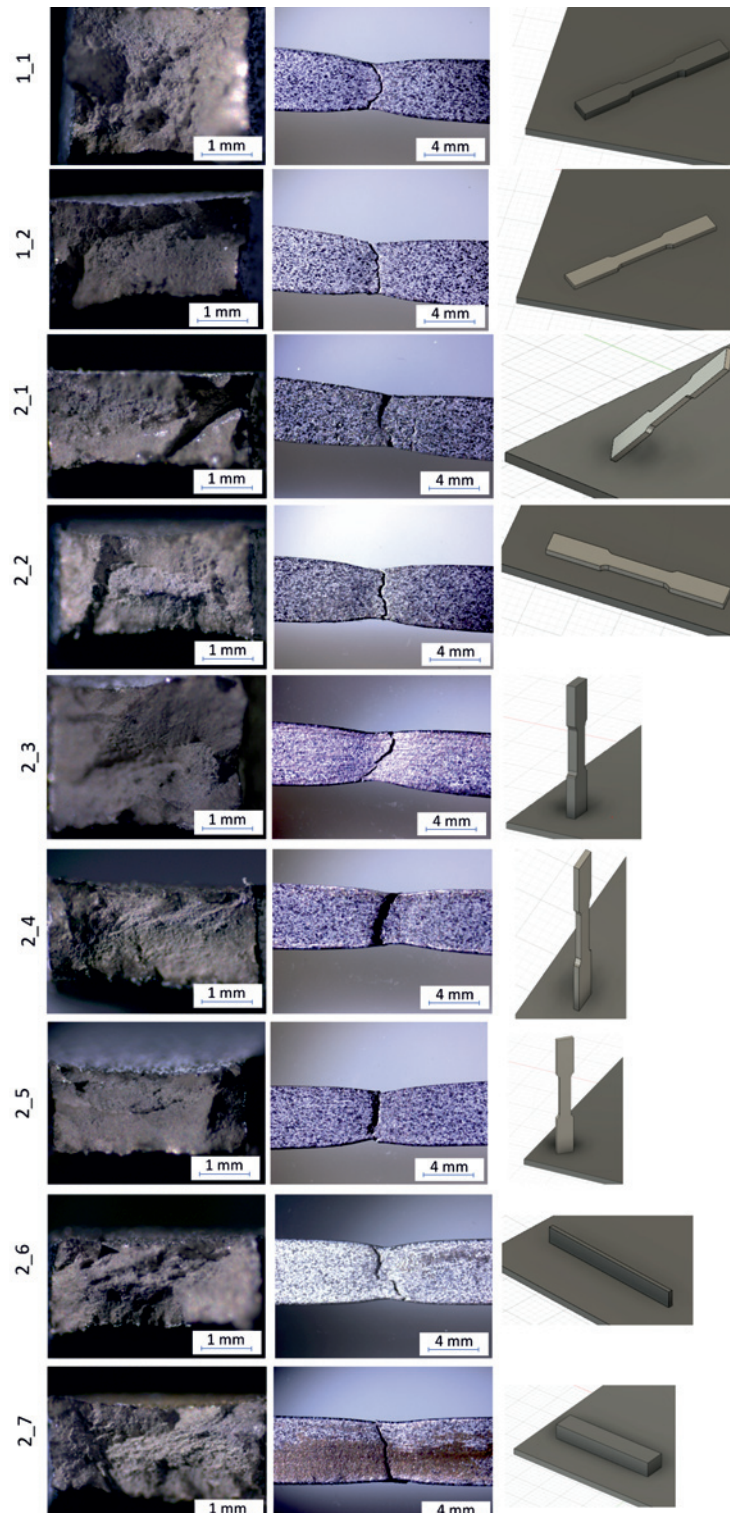


Fig. 4. Fracture surfaces of specimens observed with a stereomicroscope.

rotation with respect to the coater direction. Groups 2_3 and 1_1 have a final thickness of 5 mm, whereas 2_4 and 1_2 have a final thickness of 3 mm. As the results in Fig. 3 show, the specimen thickness does not significantly change the modulus of elasticity, yield strength, or the ultimate tensile strength taking the

standard deviations into account. However, the ductility is significantly affected by the change of the specimen thickness, as depicted in Fig. 3d with elongation at break values. The effect is even more pronounced for vertically standing specimens (Groups 2_3 and 2_4). The results show that the ductility is enhanced as the

specimen thickness becomes higher. This result is also evident from the fracture surfaces in terms of area reduction, as demonstrated in Fig. 4.

The increase of ductility concerning the thickness is attributed to the statistically higher risk of the detrimental effect of the defects in the thinner specimens. Due to the nature of this process, pores and inclusions may be found in the material, and the ratio of the total defect area to the whole cross-sections seems to be higher for thin specimens. The defect density is a critical factor determining the ductility, and as it is increased, the ductility is reduced [17]. As explained by Leicht et al., the thickness of the specimen plays a significant role in elongation to fracture due to a less favorable scatter of defects, namely pores and inclusions, in relation to the surface-to-volume ratio of the specimen. Although the porosities are more or less the same (see Section 3.2), it is possible that the deformation is localized earlier in the case of reduced load-bearing material. Moreover, the distance for a void/defect to grow to reach the surface is shorter for thinner samples. This is also encountered with conventionally manufactured specimens, as detailed in ASM Handbook [18].

Moreover, the effect of the as-built specimen geometry is tested with vertically lying specimens numbered 2.6 and 2.7. Although the as-built geometries vary in thickness for these specimens, the final thickness for these groups is taken as 3 mm. The as-built geometries vary only in one dimension, and for both sets, the specimens were built as rectangular prisms, and the final geometry was cut by WEDM from these geometries. No significant difference is observed in any of the results for these two sets, including ductility, as seen in Fig. 3.

The other process variable tested in these tensile tests was the build orientation. First of all, with no inclinations, three main build orientations are compared with group numbers of 2.2, 2.4, and 2.6. As shown in Fig. 3, vertically standing specimens (Group 2.4), of which the tension direction coincides with the build direction, exhibit a slightly lower yield strength in comparison to the other two build directions. The alignment with respect to the coater direction does not seem to significantly affect the yield strength results when the results of Groups 2.5 and 2.4 are compared, taking the standard deviations into account. Moreover, inclining the specimens (Group 2.1) does not seem to change the yield strength. The highest yield strengths are achieved by the horizontally lying coupons (Groups 2.2 and 1.2) regardless of the alignment with respect to the powder coating direction. When the ultimate tensile strengths are compared, taking the build direction into account, it is seen that the standard deviations are much less in comparison to the yield strength values. This leads to the fact that the defects in specimens are more influential on

the yield strength. The highest tensile strengths are again achieved by the coupons where the build direction is not the same as the tensile direction (Groups 2.2, 2.6, and 1.2). Inclined specimens with 45 degrees (Group 2.1) exhibit a slightly lower UTS, whereas the vertically standing coupons exhibit the lowest UTS values. The difference in the average UTS values is approximately 80 MPa, which is about 14 %, clearly showing the anisotropy as expected. Despite the variance obtained in the mechanical properties, all samples still comply with the ASTM A240M-18 standard in terms of minimum yield strength (170 MPa) and ultimate tensile strength (485 MPa) values for AISI 316L [19].

The elongation at break and Young's moduli obtained from different build orientations are shown in Figs. 3c,d. Regarding the elongation at break, in other words, ductility, vertically standing specimens generally show a higher ductility. As expected, Young's moduli are more or less the same for all tested orientations. The fracture surfaces of all specimens are shown in Fig. 3, yielding a ductile fracture with necking. There is no evident proof of any major defects, such as periodic contour porosity or inclusions, as observed by some other researchers [20].

3.2. Microstructural investigations and microhardness

The tensile specimens were investigated in terms of porosity and microstructural changes. Although the LB-PBF parameters were the same for all specimens, different porosity levels were observed at different orientations. The porosity results with their 95 % confidence interval levels and representative OM images for 5x magnification are shown in Fig. 5. Except 2.1, oriented at 45 degrees, all specimens yield a density over 99 %. Among those, horizontally built specimens (Group 1.1, Group 1.2, and Group 2.1) exhibit the highest density (99.85 % on average), while vertically built samples (Group 2.3, Group 2.4, and Group 2.5) yield the lowest density (99.52 % in average) although the variation is low. The lowest density obtained with Group 2.1 is mainly attributed to the need to use support structures beneath to ensure manufacturability. This is also in line with the findings of the Kurzynowski et al., stating that the hatch distance of support structures and their inclination angle may result in significant and periodic porosities [21]. To sum up the results, the overall porosity values do not change significantly except for the specimens needing support structures. Therefore, it can be concluded that rather than the orientation of the specimen, the need for support structures is a more dominating factor in terms of porosity, provided that the energy input is sufficient for complete melting.

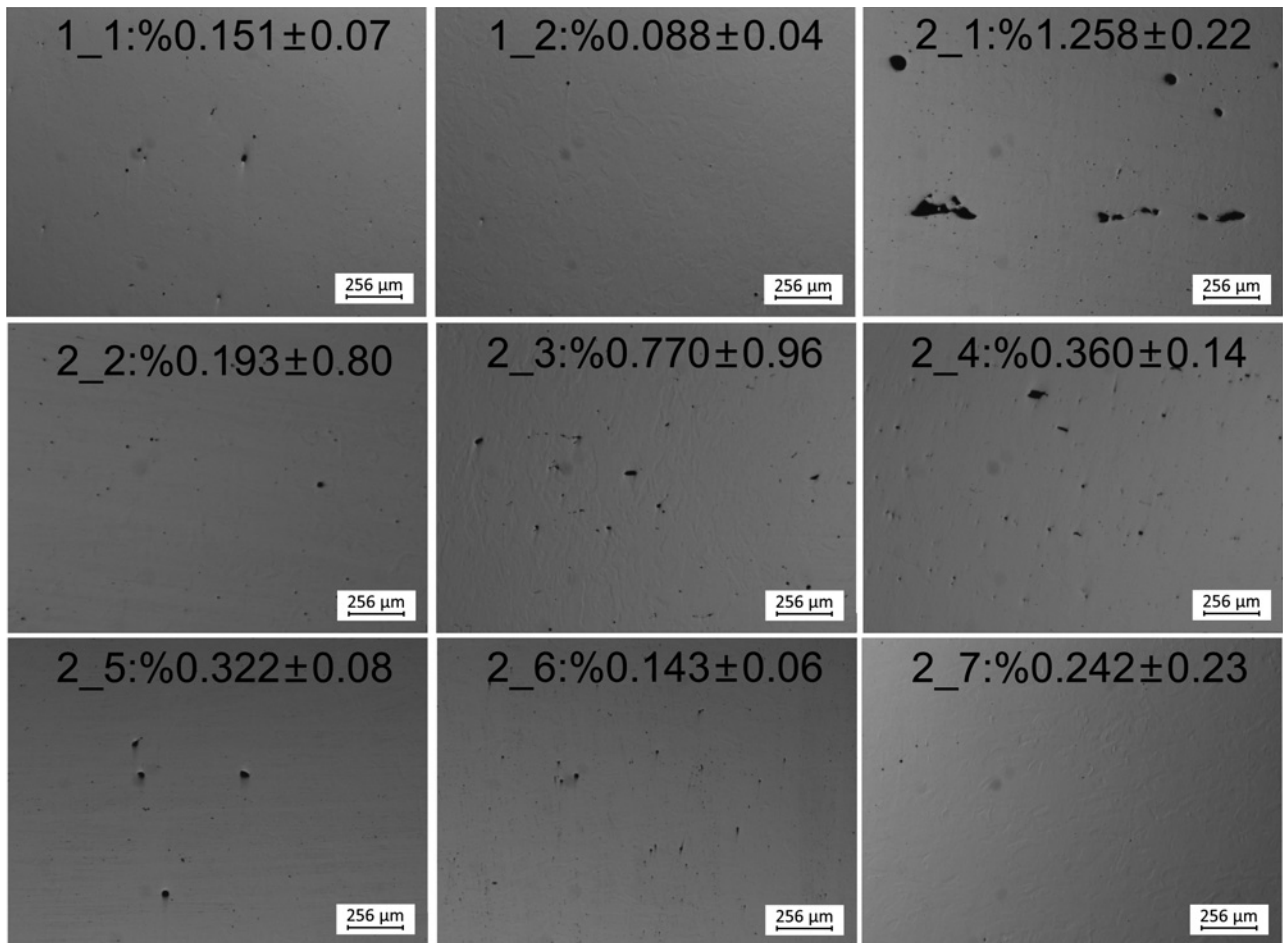


Fig. 5. Optical microscopy images of cross-section and calculated porosity levels for each specimen with 95 % confidence interval values.

Figure 6 shows the microstructure of the samples obtained with optical microscopy. It can be seen that the build direction affected grain orientation and its morphology. In vertically built samples (Groups 2.3, 2.4, and 2.5), elongated columnar grains are located parallel to the tensile direction, which may lead to lower yield and tensile strength of the samples due to lower amount of grain boundaries along the tensile direction. Similarly, vertically aligned samples (Groups 2.6 and 2.7) exhibit elongated columnar grains, and the grains are located perpendicular to the tensile direction. On the other hand, horizontally built specimens exhibit more circular grain morphology and finer grain sizes (see Fig. 7). The scan lines of horizontally built samples are also visible. Coarser grains of the horizontally built samples are located in the middle of the scan lines, and finer grains are located through the line borders. The effect of specimen thickness on the grain size of vertical samples is obvious that the higher specimen thickness yields coarser grains. However, the effect of the specimen thickness of horizontal samples is negligible. The circularity of grains also is unaffected by the specimen thickness. In the mi-

crostructure of inclined specimens (Group 2.1), neither scan lines are seen as in horizontally built samples, nor grains elongated parallel to the construction direction as observed with vertically built samples.

Figure 8 shows the variation of microhardness of the samples built in different directions showing that the variation in the hardness of all samples is negligible, taking the standard deviations into account. The average value of all specimens is about 215 HV, which is consistent with literature findings [22].

Vertically standing specimens have the lowest yield and ultimate strength among all built samples. The lowest strength values are attributed to the microstructural observations. It can be seen that columnar grains with high aspect ratios are aligned parallel to the tensile direction. This situation results in a lower amount of grain boundaries against tensile deformation. Similarly, Rickenbacher et al. obtained lower strength results for vertically built Inconel 718, and they have attributed it to grain orientation and lower amount of grain boundaries [23]. It is well known that grain boundaries behave as obstacles impeding further dislocation propagation and

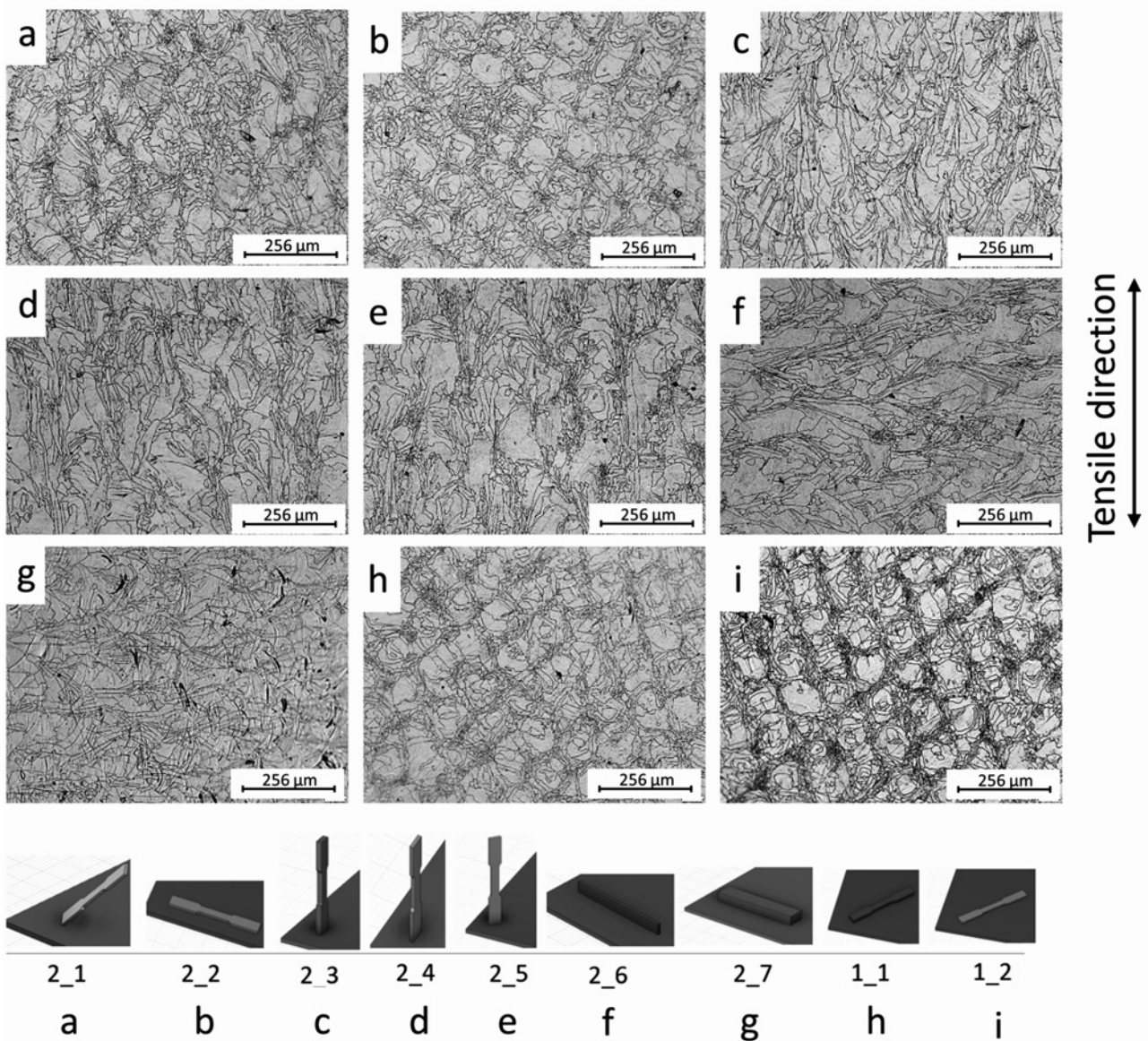


Fig. 6. Microstructure of the samples (a) 2_1, (b) 2_2, (c) 2_3, (d) 2_4, (e) 2_5, (f) 2_6, (g) 2_7, (h) 1_1, and (i) 1_2.

increasing the strength of the material. Yu et al. reported lower tensile strength and higher toughness for the vertically built orientation, attributed to different rapid solidification microstructures of AISI 316L samples along different building orientations [24]. Lower tensile strength was also reported for vertically built AISI 316L samples by other researchers [25].

4. Conclusions

The influence of the specimen geometry and build direction on the tensile properties and microstructure of AISI 316L samples produced via the LB-PBF process was investigated in this study. The significant findings can be summarized as follows:

- Almost all samples built in different orientations

yield a density over 99.5 %, whereas the specimens built with supports exhibit the highest porosity of about 1.26 %. This is attributed to the use of support structures. Thus, the need for support structures dominates the obtained density rather than the orientation.

– The final specimen thickness does not significantly affect Young's modulus, yield strength, or ultimate tensile strength, where a significant change is observed in ductility in terms of elongation at break, even at different build orientations. This is attributed to the nature of the LBPF process having some left-over porosity and the ratio of the defect area to the total cross-sectional area. This result is consistent with the findings of Laursen et al., stating that the material ductility exhibited a strong linear relationship to the sample porosity in contrast to yield strength, ultimate

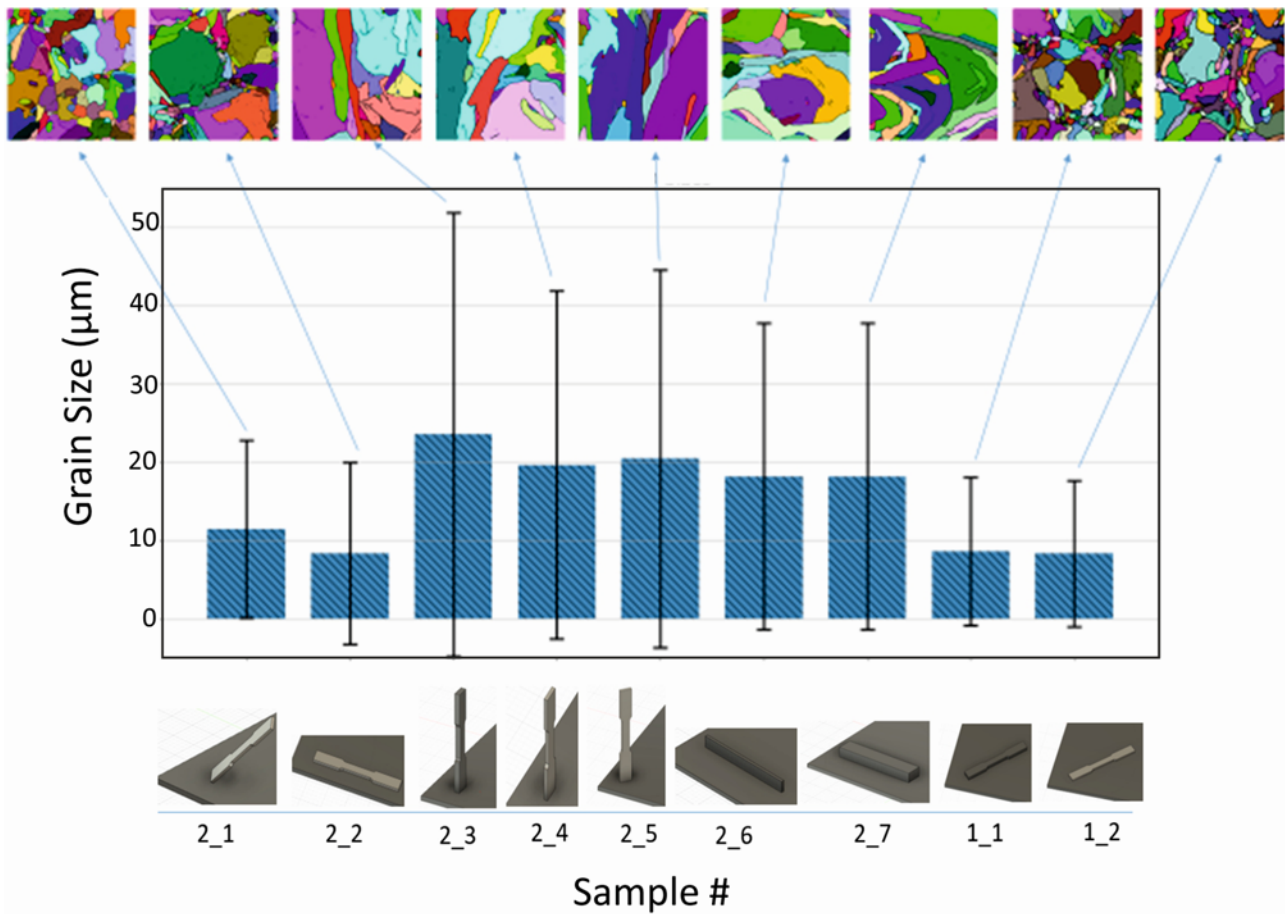


Fig. 7. Grain sizes of the samples.

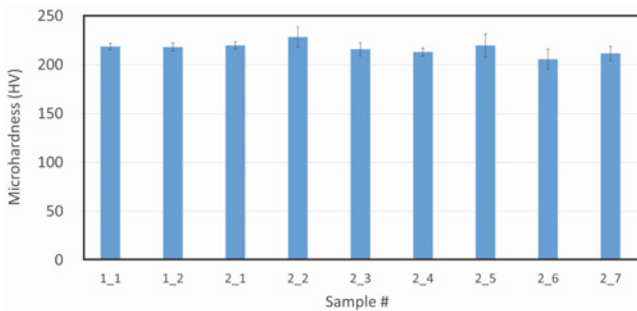


Fig. 8. Hardness measurement results with 95 % confidence intervals.

tensile strength, and elasticity modulus [26].

– While vertically standing samples have the lowest yield and ultimate tensile strength values, horizontally built samples output the highest strength values due to microstructural effects. The strength of the inclined specimens lies in between.

– The Young's modulus, found to vary between 170–200 GPa in this study, does not change significantly with respect to the specimen geometry and build orientation.

– Despite the variance obtained in the mechanical properties, all samples still comply with the ASTM A240M-18 standard in terms of minimum yield strength (170 MPa) and ultimate tensile strength (485 MPa) values for AISI 316 L.

Microhardness values change between 210–225 HV, and the build direction and the specimen geometry do not significantly affect the obtained microhardness.

Acknowledgements

This work was financially supported by FNSS Savunma Sistemleri A.Ş. The authors would like to thank Dr. Kivılcım Ersoy and Barış Koç for their special attention to this work.

References

- [1] C. Y. Yap, C. K. Chua, Z. L. Dong, Z. H. Liu, D. Q. Zhang, L. E. Loh, S. L. Sing, Review of selective laser melting: Materials and applications, *Appl. Phys. Rev.* 2 (2015) 041101. [doi:10.1063/1.4935926](https://doi.org/10.1063/1.4935926)
- [2] J. Zhang, B. Song, Q. Wei, D. Bourell, Y. Shi, A review of selective laser melting of aluminum alloys:

- processing, microstructure, property and developing trends, *J. Mater. Sci. Technol.* 35 (2019) 270–284. [doi:10.1016/j.jmst.2018.09.004](https://doi.org/10.1016/j.jmst.2018.09.004)
- [3] P. K. Gokuldoss, S. Kolla, J. Eckert, Additive manufacturing processes: selective laser melting, electron beam melting and binder jetting-selection guidelines, *Materials* 10 (2017) 672. [doi:10.3390/ma10060672](https://doi.org/10.3390/ma10060672)
- [4] J.-P. Kruth, S. Dadbakhsh, B. Vrancken, K. Kempen, J. Vleugels, J. Van Humbeeck, Additive Manufacturing of Metals via Selective Laser Melting Process Aspects and Material Developments. In: T. S. Srivatsan and T. S. Sudarshan (Eds.), *Additive Manufacturing: Innovations, Advances, and Applications*, CRC Press, New York, 2016, pp. 69–99.
- [5] F. Trevisan, F. Calignano, M. Lorusso, J. Pakkanen, A. Aversa, E. P. Ambrosio, M. Lombardi, P. Fino, D. Manfredi, On the selective laser melting (SLM) of the AlSi10Mg alloy: Process, microstructure, and mechanical properties, *Materials* 10 (2017) 76. [doi:10.3390/ma10010076](https://doi.org/10.3390/ma10010076)
- [6] I. Yadroitsev, I. Smurov, Selective laser melting technology: From the single laser melted track stability to 3D parts of complex shape, *Phys. Procedia* 5 (2010) 551–560. [doi:10.1016/j.phpro.2010.08.083](https://doi.org/10.1016/j.phpro.2010.08.083)
- [7] E. Liverani, S. Toschi, L. Ceschini, A. Fortunato, Effect of selective laser melting (SLM) process parameters on microstructure and mechanical properties of 316L austenitic stainless steel, *J. Mater. Process. Technol.* 249 (2017) 255–263. [doi:10.1016/j.imatprotec.2017.05.042](https://doi.org/10.1016/j.imatprotec.2017.05.042)
- [8] C. S. Rakesh, N. Priyanka, R. Jayaganthan, N. J. Vasa, Effect of build atmosphere on the mechanical properties of AlSi10Mg produced by selective laser melting, *Mater. Today: Proc.* 5 (2018) 17231–17238. [doi:10.1016/j.matpr.2018.04.133](https://doi.org/10.1016/j.matpr.2018.04.133)
- [9] J. T. O. de Menezes, E. M. Castrodeza, R. Casati, Effect of build orientation on fracture and tensile behavior of A357 Al alloy processed by Selective Laser Melting, *Mater. Sci. Eng. A* 766 (2019) 138392. [doi:10.1016/j.msea.2019.138392](https://doi.org/10.1016/j.msea.2019.138392)
- [10] S. Ren, Y. Chen, T. Liu, X. Qu, Effect of build orientation on mechanical properties and microstructure of Ti-6Al-4V manufactured by selective laser melting, *Metall. Mater. Trans. A* 50 (2019) 4388–4409. [doi:10.1007/s11661-019-05322-w](https://doi.org/10.1007/s11661-019-05322-w)
- [11] A. Röttger, J. Boes, W. Theisen, M. Thiele, C. Esen, A. Edelmann, R. Hellmann, Microstructure and mechanical properties of 316L austenitic stainless steel processed by different SLM devices, *Int. J. Adv. Manuf. Technol.* 108 (2020) 769–783. [doi:10.1007/s00170-020-05371-1](https://doi.org/10.1007/s00170-020-05371-1)
- [12] H. H. Alsalla, C. Smith, L. Hao, Effect of build orientation on the surface quality, microstructure and mechanical properties of selective laser melting 316L stainless steel, *Rapid Prototyp. J.* 24 (2018) 9–17. [doi:10.1108/RPJ-04-2016-0068](https://doi.org/10.1108/RPJ-04-2016-0068)
- [13] T. Taufek, Y. HP Manurung, S. Lueder, Z. Mingu, F. HS Pengadai, Metallurgical and structural investigation on SS316L specimens manufactured by additive manufacturing using SLM, *Int. J. Eng. Technol.* 7 (2018) 1608–1612.
- [14] J. Delgado, J. Ciurana, C. A. Rodríguez, Influence of process parameters on part quality and mechanical properties for DMLS and SLM with iron-based materials, *Int. J. Adv. Manuf. Technol.* 60 (2012) 601–610. [doi:10.1007/s00170-011-3643-5](https://doi.org/10.1007/s00170-011-3643-5)
- [15] ASTM E8/E8M-16a: Standard Test Methods for Tension Testing of Metallic Materials, West Conshohocken, PA, USA: ASTM International (2016).
- [16] ASTM E92-17, Standard Test Methods for Vickers Hardness and Knoop Hardness of Metallic Materials, West Conshohocken (PA): ASTM International (2017).
- [17] M. Jaskari, S. Ghosh, I. Miettunen, P. Karjalainen, A. Järvenpää, Tensile properties and deformation of AISI 316L additively manufactured with various energy densities, *Materials* 14 (2021) 5809. [doi:10.3390/ma14195809](https://doi.org/10.3390/ma14195809)
- [18] G. T. Gray, H. Kuhn, D. Medlin, *ASM Handbook Vol. 8: Mechanical Testing and Evaluation*. ASM International, Materials Park 2000. ISBN: 0-87170-389-0
- [19] ASTM A240/A240M-18: Standard Specification for Chromium and Chromium-nickel Stainless Steel Plate, Sheet, and Strip for Pressure Vessels and for General Applications, West Conshohocken (PA): ASTM International (2018)
- [20] K. Solberg, S. Guan, S. M. J. Razavi, T. Welo, K. C. Chan, F. Berto, Fatigue of additively manufactured 316L stainless steel: The influence of porosity and surface roughness, *Fatigue Fract. Eng. Mater. Struct.* 42 (2019) 2043–2052. [doi:10.1111/ffe.13077](https://doi.org/10.1111/ffe.13077)
- [21] T. Kurzynowski, W. Stopyra, K. Gruber, G. Ziolkowski, B. Kuźnicka, E. Chlebus, Effect of scanning and support strategies on relative density of SLM-ed H13 steel in relation to specimen size, *Materials* 12 (2019) 239. [doi:10.3390/ma12020239](https://doi.org/10.3390/ma12020239)
- [22] A. M. Roach, B. C. White, A. Garland, B. H. Jared, J. D. Carroll, B. L. Boyce, Size-dependent stochastic tensile properties in additively manufactured 316L stainless steel, *Addit. Manuf.* 32 (2020) 101090. [doi:10.1016/j.addma.2020.101090](https://doi.org/10.1016/j.addma.2020.101090)
- [23] L. Rickenbacher, T. Etter, S. Hövel, K. Wegener, High temperature material properties of IN738LC processed by selective laser melting (SLM) technology, *Rapid Prototyp. J.* 19 (2013) 282–290. [doi:10.1108/13552541311323281](https://doi.org/10.1108/13552541311323281)
- [24] A. Sharma, M. C. Oh, J.-T. Kim, A. K. Srivastava, B. Ahn, Investigation of electrochemical corrosion behavior of additive manufactured Ti-6Al-4V alloy for medical implants in different electrolytes, *J. Alloys Compd.* 830 (2020) 154620. [doi:10.1016/j.jallcom.2020.154620](https://doi.org/10.1016/j.jallcom.2020.154620)
- [25] N. Lavery, J. Cherry, S. Mehmood, H. Davies, B. Girling, E. Sackett, S. Brown, J. Sienz, Effects of hot isostatic pressing on the elastic modulus and tensile properties of 316L parts made by powder bed laser fusion, *Mater. Sci. Eng. A* 693 (2017) 186–213. [doi:10.1016/j.msea.2017.03.100](https://doi.org/10.1016/j.msea.2017.03.100)
- [26] C. M. Laursen, S. A. DeJong, S. M. Dickens, A. N. Exil, D. F. Susan, J. D. Carroll, Relationship between ductility and the porosity of additively manufactured AlSi10Mg, *Mater. Sci. Eng. A* 795 (2020) 139922. [doi:10.1016/j.msea.2020.139922](https://doi.org/10.1016/j.msea.2020.139922)